Subcellular Localization of the P2X4 Receptor in Cochlear Sensory Hair Cells

Ziyin Silver Huang
The University of Auckland
Jacqueline M Ross
The University of Auckland
Shelly CY Lin
The University of Auckland
Kevin Roy
The University of Auckland
Srdjan M Vlajkovic
The University of Auckland
Peter R. Thorne
The University of Auckland
Haruna Suzuki-Kerr
h.suzuki-kerr@auckland.ac.nz
The University of Auckland

Research Article

Keywords: Cochlea, sensory hair cell, purinergic signalling, P2X receptor, P2X4, ATP, Organ of Corti

Posted Date: June 6th, 2024

DOI: https://doi.org/10.21203/rs.3.rs-4474581/v1

Additional Declarations: No competing interests reported.

Version of Record: A version of this preprint was published at Histochemistry and Cell Biology on May 20th, 2025. See the published version at https://doi.org/10.1007/s00418-025-02386-1.

Abstract

Our sense of hearing starts in the inner ear organ, the cochlea, which contains two types of auditory hair cells for signal transduction. Earlier research showed that the complex cochlear physiology is regulated in part by purinergic signalling through activations of purine mediated P2X, P2Y and adenosine receptors expressed in the cochlea. This study aims to extend our knowledge of purinergic signalling in the cochlea by comprehensively characterizing the expression of $P2X_4$ receptor subtype. Wistar rat cochlea (embryonic day 20.5–6 weeks, both sexes) were collected and the $P2X_4$ expression was examined by immunohistochemistry. Robust $P2X_4$ expression was found in the organ of Corti (OoC) in the inner hair cells (IHCs) and outer hair cells (OHCs), confirmed by double-labelling with HCs marker Myosin VIIa. In IHCs, a robust cytoplasmic $P2X_4$ expression occurred throughout the cell body, with the most intense signal at the medial side. In OHCs, $P2X_4$ formed puncta near the apical and basal ends of the cell body. Using markers for subcellular organelles, P2X4 immunoreactivity was associated mostly with the trans-Golgi network apparatus (27%) and early endosomes (26%) in IHC, and early endosomes (42.3%) and lysosomes (32.4%) in OHC in the mature cochlea. Taken together, these observations suggest unique roles for $P2X_4$ in mature IHCs and OHCs as a purinergic receptor subtype responsible for homeostatic regulation of hair cells and auditory sensory transduction.

INTRODUCTION

According to the World Report on Hearing (2021), hearing loss affects 1.5B people globally and this number is expected to grow to 2.5B by 2050 (World Health Organization, 2021). The majority of cases are sensorineural hearing loss (SNHL), characterized by degenerative changes in the cochlea and the auditory nerve. There are few effective pharmacological treatments for SNHL and development of such treatment requires further understanding of cochlear physiology and pathophysiology at the cellular and molecular levels. The organ of Corti (OoC), the sensory apparatus within the cochlea, contains two types of auditory sensory cells, the inner hair cells (IHC) and outer hair cells (OHC). Hair cells (HCs) are so-called due to mechanosensory stereocilia located on the apical side of the cell supported by an actin-rich cuticular plate and are essential for sound transduction (Goodyear, Marcotti, Kros, & Richardson, 2005). Approximately 3500 IHCs are aligned as a single continuous row and 12,000 OHCs arranged in three rows more laterally in the human cochlea. In humans and animal models, loss of HCs, particularly OHC and loss of synapses and neurons innervating IHC have been observed as a common underlying pathology associated with SNHL (Liberman & Kujawa, 2017-z. Wu, O'Malley, de Gruttola, & Liberman, 2020; P. Z. Wu et al., 2019).

Purinergic signaling is involved in many cellular functions and pathologies in the inner ear and considered to be a potential therapeutic target for inner ear disorders. Purinergic signaling pathways are activated by extracellular nucleotides adenosine triphosphate (ATP), adenosine diphosphate (ADP), uridine triphosphate (UTP), uridine diphosphate (UDP), and adenosine (Burnstock, 1997). There are two classes of purinergic receptors: P1 receptors (A_1, A_{2A}, A_{2B} and A_3) and P2 receptors ($P2X_{1\text{-}7}$, $P2Y_{1,2,4,6,\ 11\text{-}14}$) (Burnstock, 2007). Many of these purinoceptor subtypes have been identified in the cochlea (Köles, Szepesy, Berekméri, & Zelles, 2019; Vlajkovic & Thorne, 2022). P2X receptors form trimeric ligand-gated ion channels that are non-selectively permeable to cations (Na^+, K^+, Ca^{2+}) (Burnstock, 2007). Earlier studies had suggested a potential role for P2X receptors in the cochlea, such as regulation of afferent neuronal activity in response to agonists released in

the perilymph (Robertson & Paki, 2002). More specific roles for P2X subtypes are emerging based on molecular and functional investigations; $P2X_2$ expressed in cells lining the endolymphatic compartment and in the stereocilia of OHC participate in the reduction of endocochlear potential during sound transduction and in modulating the sound sensitivity, respectively (Jarlebark, Housley, & Thorne, 2000; Morton-Jones et al., 2015; Z.-J. Wang & Neuhuber, 2003). $P2X_1$ and $P2X_7$ localized near synaptic terminals of the auditory neurons on IHCs and in the neurites of the SGN (P. Nikolic, Housley, Luo, Ryan, & Thorne, 2001; Predrag Nikolic, Housley, & Thorne, 2003) may play roles in Ca^{2+}-dependent uncoupling of synapses known to occur at these postsynaptic terminals (Liberman & Kujawa, 2017). $P2X_3$ expressed in the developing spiral ganglion neurons regulate branching of afferent fibres (L.-C. Huang, Ryan, Cockayne, & Housley, 2006; Z. Wang et al., 2020). In contrast, molecular expression of $P2X_{4-6}$ has not been clearly demonstrated in the cochlea. $P2X_4$ has some unique features compared to other P2X subtypes. The human monomeric $P2X_4$ channel is sensitive to the extracellular Ca^{2+} concentration with slow desensitization compared to $P2X_{1-3}$ isoforms requiring 4 sec at a 30μM concentration ATP (Hattori & Gouaux, 2012). Cytoplasmic expression of $P2X_4$ and localization to lysosomes have been reported (Huang et al., 2014; Murrell-Lagnado & Frick, 2019). Intracellular $P2X_4$ exhibit pH sensitivity (inactivated at low pH) and can be regulated by the pH within the lysosomal lumen (P. Huang et al., 2014; Ruth D. Murrell-Lagnado & Frick, 2019). In the guinea pig cochlea, functional expression of $P2X_4$ has been reported in the endothelial cells of the spiral ligament where it appears to regulate cochlear blood flow (Y. Wu et al., 2011) and in hair cells (Szücs et al., 2004), however, the detailed $P2X_4$ distribution in the cochlea still remains to be characterized. In the vestibular system of the inner ear, $P2X_4$ molecular and functional expression has recently been reported in vestibular supporting cells (Jeong et al., 2020).

In this study, we investigated the distribution of $P2X_4$ in the developing and adult rat cochlea. Expression was confined to OHCs and IHCs, and located solely in the cytoplasm. Colocalization with markers of endoplasmic reticulum, Golgi apparatus and lysosomes suggests that $P2X_4$ is associated with different intracellular organelles (Golgi-ER in IHC and lysosomes in OHC) and may mediate calcium buffering within these intracellular organelles.

METHOD AND MATERIALS

Animals

The use of animals for this project was approved by the University of Auckland Animal Ethics Committee (AEC002251). All animals were supplied by the Vernon Jensen Unit (VJU; The University of Auckland). Wistar rats of various ages and both sexes were used for this study; embryonic day 20.5, postnatal day 4 (P4), postnatal day 8 (P8), postnatal day 21 (P21), and 6-week-old (adult).

Tissue preparation

General chemicals were purchased from ThermoFisher Scientific (Auckland, New Zealand) unless otherwise specified. 4% w/v Paraformaldehyde (PFA, pH 7.4) was prepared with 0.1M Phosphate Buffer (PB, 24.6 mM NaH_2PO_4 and 75.4 mM $NaHPO_4$, pH 7.4) for fixation of all samples. P21 and adult rats were first anaesthetised

and euthanized by drug overdose (Pentobarbital, ProVet NZ Pty Ltd), followed by perfusion of 0.1% w/v $NaNO_2$ in Phosphate-Buffered Saline (PBS, pH 7.4, Gibco), and 4% PFA through the left ventricle. The temporal bones were removed from the cranium and a small puncture was carefully made in the round window membrane to aid the penetration of PFA into the cochlea. The cochlea was then immersion fixed in 4% PFA at room temperature (RT) for 24 hours. Cochleae were washed with PBS three times (10 mins each). Adult cochlear tissues were decalcified by immersion in 4% w/v Ethylenediaminetetraacetic acid (EDTA, in 0.1PB, pH 7.4) at room temperature for up to 2 weeks with regular change of EDTA solution. Cochleae from Wistar rats younger than P8 were removed and immersed in PFA (4% PFA at room temperature (RT)) for 24 hours and further dissection was carried out without decalcification. For the organ of Corti (OoC) whole mount preparations, cochleae were micro-dissected in PBS and segments of OoC approximately equivalent to ½ turn, were taken from the apical, middle, and basal turn. For cryosectioning, cochleae were cryoprotected sequentially in 10% and 20% sucrose (w/v in PBS) for one hour at room temperature, then in 30% sucrose overnight at 4°C followed by embedding in Tissue-Tek Optimal Cutting Temperature Compound (OCT, ProSciTech, Australia) at -80°C. The tissue was cryosectioned at 20-30 mm (Leica, CM3050S) in the axial plane through the modiolus and cochlear ducts. Microdissected or cryosectioned tissue was stored in PBS for up to 1 week at 4°C before processing for immunohistochemistry.

Immunohistochemistry

The list of primary antibodies used in this study and dilutions are summarised in Table 1. A polyclonal primary antibody raised in rabbits against the C-terminal domain of the rat $P2X_4$ subunit (Alomone Inc., Jerusalem, Israel, catalogue no. APR-002) was used for detection of $P2X_4$ by immunohistochemistry. This antibody has been validated using $P2X_4$ knockout animals (Lalisse et al., 2018; Sim et al., 2006; Wyatt et al., 2014). Other antibodies used as cell-type specific markers and organelle markers are summarized in Table 1. Immunohistochemistry was performed following the protocol established previously (Fok et al., 2020; Han, Lin, Espinosa, Thorne, & Vlajkovic, 2019). Blocking solutions and antibody diluent solutions were prepared as following; blocking solution for whole mounts (10% v/v normal goat serum (NGS) and 2.5% (v/v) TritonX in PBS), blocking solution for cryosection (10% v/v NGS, 1% v/v TritonX in PBS), antibody diluent for wholemount (5% v/v NGS and 0.25% v/v TritonX in PBS) and antibody diluent for cryosection (5% v/v NGS and 0.1% v/v TritonX in PBS). Tissues were incubated for 2 hours in a blocking solution at room temperature. Tissues were then incubated in the diluted primary antibody overnight at 4℃°. For the anti-$P2X_4$ antibody control, the pre-absorbing peptide was added to the primary antibody solution in a 1mg-1mg ratio and sections or whole mounts were incubated for 2 hours following the manufacturer's protocol (Alomone Labs, Israel). Tissues were washed 4 times at 1, 10, 15, 30 minutes intervals in PBS at RT followed by incubation with secondary antibodies overnight at 4°C in the dark. Secondary antibodies used were goat anti-rabbit Alexa Fluor 594, goat anti-rabbit Alexa Fluor 488, and goat anti-mouse Alexa Fluor 647 (ThermoFisher Scientific, all used at 1:500 dilution in antibody diluent). The non-antibody labelling reagents Wheat Germ Agglutinin (WGA) and Phalloidin (Table 1) were included in the same mixture with the secondary antibody. From this step forward, tissues were covered to minimize light exposure. After incubation with secondary antibodies, the tissues were washed 4 times in PBS, incubated in DAPI (diluted in PBS, 0.02mg/ml) for an hour at room temperature, washed 4 times

in PBS and mounted with coverslips on slides with CitiFluor AF1 mountant solution (Agar Scientific Ltd, UK). Slides were stored at 4°C in the dark until imaging.

Confocal microscopy

Fluorescently immunolabelled slides were imaged using a Zeiss LSM 800 Airyscan confocal microscope (Carl Zeiss GmbH, Jena, Germany) in the Biomedical Imaging Research Unit (BIRU) at The University of Auckland. Objective lenses used were 10x/0.45 NA Plan Apochromat, 20x/0.8 NA Plan Apochromat, 63x/1.4 NA Plan Apochromat oil immersion. Images were acquired at a pixel resolution of 0.18µm/pixel for 20x, and 0.035µm/pixel for 63x in Airyscan mode. The Z series were obtained using a 63x/1.4 NA oil immersion objective lens with a 0.5mm step size between optical sections. The top limit for the Z series was set at the level of the tip of the stereocilia of the hair cells, as visualized with phalloidin representing the most apical end of the cell body, and the bottom limit was set at the opposite end of the hair cell body at the position where the $P2X_4$ signal had just disappeared from the HCs. A typical Z-stack was 40mm thick. All of the images were acquired using ZEN 2.6 software (Carl Zeiss, Germany) and exported to TIFF as required for figure preparation or analysis.

Image analysis and processing

ImageJ (Schneider et al., 2012) was used for particle analysis and quantification of $P2X_4$ immunolabeling on individual cells from the z series images (see Supplementary material for details on methodology). An automated threshold was used to identify the particles of interest. The measurements were then carried out using the built-in Particle Analyzer. Parameters included “Count” and “Total Area”. “Count” represents the number of particles in each image and “Total Area” is the area represented by the sum of the particles in each image. ImageJ “line plot profile” analysis was performed to quantify the relative signal intensity within the hair cells in apical to basal direction. This function was also used to measure intensity at nine different locations in the hair cell across the apical-basal as well as medial-lateral directions and normalised relative to the total signal (Figure 3 & 4 and Supplementary Figure 1). The JACoP plugin (see Supplementary material for more detail) was used for colocalization analysis between $P2X_4$ and subcellular markers. Individual channels were separately processed by background subtraction and images were cropped so that the region of interest typically contained 8 cells. JACoP automatically calculates Manders’ colocalization coefficients (with and without a threshold) and Pearson’s correlation coefficient (Bolte & Cordelières, 2006; Dunn, Kamocka, & McDonald, 2011). The results were displayed as M1 and M2, each with the value range between 0-1.0, where M1 is defined as the ratio of the “summed intensities of pixels from the green channel for which the intensity in the red channel is above zero” to the “total intensity in the green channel”. M2 is identified as the same as the red and green reversed. High M1 and M2 coefficients indicate that a large proportion of one signal co-occurs with the other signal. Colocalization analyses were conducted for each subcellular marker separately, with 3 cochleae for each marker, and the mean and standard error of the mean (SEM) were calculated. Imaging processing was performed using Adobe Photoshop CC (version 19.1.3, Adobe system Incorporated) to prepare figures.

RESULTS

$P2X_4$ expression in the cochlea

After testing the dilution range 1:50 to 1:2000, 1:1000 dilution was chosen to have the best signal to background ratio (data not shown) for the anti-$P2X_4$ antibody (Figure 1). High levels of expression of $P2X_4$ in the rat OoC were observed (Figure 1D, F), but less in the spiral ligament (Figure 1C, arrow) and spiral ganglion (Figure 1E, arrow) In the OoC, there was a relatively higher expression in IHC & and to a lesser extent in OHCs (Figure 1D, F-H). Immunolabeling of P2X4 throughout was abolished by preabsorbing $P2X_4$ antibody with excess peptide molecules in the controls (Figure 1I). The expression of $P2X_4$ was evident in the hair cells from E20.5 but was more prominent in the IHCs than OHCs. When compared the OoC at different rat ages,(E20.5, P4, P8, P21); Figure C-F), immature IHC at E20.5 expressed P2X4 above the background, but the signal was relatively weak. At P4 and P8, expression of $P2X_4$ was clearly evident in IHCs and OHCs. By P21, a week after the hearing onset, $P2X_4$ exhibited a similar expression pattern to the adult cochlea with strong expression of $P2X_4$ in the IHCs. At P8, $P2X_4$ expression was prominent in IHC & OHC (Figure 2A-B). Some cells lining the cochlear scala tympani and vestibuli also expressed detectable levels of $P2X_4$ (Figure 2A-B, arrows). It is not possible to identify these cells but they appear morphologically very similar to Iba1-expressing macrophages observed in the postnatal mouse cochlea (Kishimoto, Okano, Nishimura, Motohashi, & Omori, 2019). To confirm the identity of cells expressing $P2X_4$, two cell-type specific markers were used: myosin VIIa, which is consistently expressed in IHC and OHCs (Jung et al., 2019; Xiong et al., 2019) and Sox2, which is a transcription factor expressed in nuclei of all types of supporting cells (Smeti et al., 2011). $P2X_4$-labelled cells co-expressed myosin VIIa, confirming these to be the IHCs and OHCs (Figure 2G), while $P2X_4$ was not observed in cells expressing Sox2 (Figure 2H).

Polarity of $P2X_4$ subcellular distribution within IHC and OHC in adult rat cochlea

We next investigated the subcellular localizations of IHCs and OHCs in the adult rat cochlea to correlate the distribution of $P2X_4$ with the distinct functional domains of IHC and OHC. Analysis of z-stack images of OoC enabled compartmentalisation of the hair cells into four different sub-domains from the apical surface to the basal pole of the cell; sub-cuticular (Figure 3A), cytoplasmic (Figure 3B), nuclear (Figure 3C) and subnuclear zones (Figure 3D). At the sub-cuticular plate level of IHC, $P2X_4$ immunolabeling appeared as bright irregular clusters in the cell cytoplasm immediately underneath the cuticular plate (Figure 3A). In the supranuclear cytoplasm, between the cuticular plate and nucleus, there were similar clusters of $P2X_4$ immunolabelling, but these appeared larger and brighter (Figure 3B). At the nucleus and sub-nucleus levels, the cytoplasmic immunolabeling for $P2X_4$ appeared brightest and the most abundant (Figure 3C, D). This pattern is also evident in the 3D re-constructions (Figure 3E). Orthogonal views of the images were also generated with ImageJ where the stack of images was viewed in a XY, YZ, XZ planes, where the X, Y, Z planes correspond to the left and right (Le-R), medial and lateral (M-L) and the apical and basal (A-B), respectively (Figure 3F). Orthogonal visualization confirmed more intense $P2X_4$ immunolabeling along the medial side of the IHCs

(Figure 3F", arrow). This corresponds to the large, patchy signal appearance in the 3D re-construction (Figure 3E). More intense signal was also observed at the apical part of the image (Figure 3F"'). Signal distribution for $P2X_4$ along the apical-basal and medial-lateral axes of the cells was quantified using ImageJ (Supplementary Figure 4) to confirm these visual observations that the $P2X_4$ expression was more concentrated at the basal end of the IHCs (Figure 3G) and at the medial side of the IHCs (Figure 3H).

Similar analyses in the OHCs (Figure 4) showed $P2X_4$ immunolabeling at all four levels predominately in the cell cytoplasm, however the characteristic pattern of $P2X_4$ localisation was quite different from that observed in IHCs. At the sub-cuticular plate level, the $P2X_4$ expression appeared to be more concentrated than observed in IHC (Figure 4A). Interestingly, the cluster of $P2X_4$ labelling often appeared immediately underneath the 'cuticular-free zone', a small region on the lateral aspect of the cell that does not stain with phalloidin (Figure 4 arrow). At the cytoplasmic level, regions of P2X4 appeared more scattered, but some medium-sized clusters were observed (Figure 4B). At the nucleus level, the $P2X_4$ immunoreactivity was less obvious (Figure 4C), but more intense in the basal sub-nucleus level of OHC (Figure 4D). When reconstructed in 3D, a prominent cluster of $P2X_4$ immunolabeling was observed at the apical part of the cytoplasm, and it was not as homogenously distributed through the whole cell compared to $P2X_4$ immunolabeling in IHC (Figure 4E). Examined using the orthogonal view, the most intense signal for $P2X_4$ (Figure 4F", asterisks), appearing as a prominent cluster, was observed at the lateral side of each cell underneath the CP free zone (Figure 4E). Z-stack images obtained for the OHCs were quantified using ImageJ (See supplementary figure 5 for details) to confirm that the $P2X_4$ expression was more concentrated at both the apical and the basal end of the OHCs (Figure 4G). The gradient in OHC was very subtle in the medial to lateral direction (Figure 4L-M), compared to the clear trend observed for IHC (Figure 3H). Immunolabeling for of $P2X_4$ appeared as more discrete dots in the OHCs compared to the IHCs, allowing additional "particle analysis" (Figure 5A & B; see Supplementary Figure 3 for more detail). The total area occupied by $P2X_4$ immunolabeling was the greatest in the sub-cuticular zone, compared to the three other zones (Figure 5C). In contrast, the total amount of staining was the highest in the cytoplasmic zone compared to the other three zones (Figure 5D).

Localization of $P2X_4$ to subcellular organelles within IHCs and OHCs.

The $P2X_4$ immunostaining was in clusters and appeared to be vesiculated. To determine if these were associated with other membranous intracellular organelles, we looked at co-localisation of $P2X_4$ with endosomes, lysosomes, Golgi bodies and mitochondria using immunohistochemistry (Table 1). Early endosomes are derived from the plasma membrane (Gindhart & Weber, 2009) and distinguished from late endosomes and other vesicles by the expression of early endosome antigen 1 (EEA-1) (Patki et al., 1997), including in IHCs and OHCs (Schug et al., 2006). Endosomes and the Golgi apparatus are part of the intracellular protein transportation and recycling pathway. EEA-1 labelling in IHCs had a diffuse appearance, with vesicular labelling more concentrated in the apical part of the cell (Figure 6A). In OHCs, EEA-1 labelled vesicles appeared throughout (Figure 6B). There was some co-labelling between EEA-1 and $P2X_4$ (Figure 6A, B arrow) in both IHC and OHC, with qualitatively more co-occurrence observed in OHC. To quantify the co-

localization of EEA-1 with $P2X_4$, the JACoP plugin (Bolte & Cordelières, 2006) in ImageJ was used (see Supplementary Figure 3 for details). Z-stack images covering either entire OHCs or IHCs were selected for analysis. JACoP quantifies the co-occurrence of $P2X_4$ and EEA-1 as two "Mander's coefficients" calculated as M1 and M2 coefficients with a value range between 0-1.0. M1 represents the proportion of EEA-1 co-localized with $P2X_4$ signal over the total $P2X_4$ signal. M2 represents the proportion of the EEA-1 co-localized with $P2X_4$ over the total signal of EEA-1. The average M1 values for each organelle marker in IHC and OHC are summarised in Figure 6J & K.

Taking the same approach, we analysed the co-occurrence of $P2X_4$ with LAMP-1, GM130, Tom20 and Wheat Germ Agglutinin (WGA). LAMP-1 is a protein found on lysosomes and lysosome-endosome fusion vesicles and is commonly used as a marker for lysosomes (Huotari & Helenius, 2011). Lysosomes are distributed throughout the cell in the IHCs and OHCs, but large lysosomes are often found at the apical, lateral side of the cell (Spicer, Thomopoulos, & Schulte, 1999). OHCs have a greater number of lysosomes compared to IHCs (Spicer, Thomopoulos, & Schulte, 1998; Wiwatpanit et al., 2018). LAMP-1 labelling in IHCs had a more diffuse appearance with lower signal levels, and minimally co-occurred with $P2X_4$ (Figure 6C) where the OHCs had a vesicular appearance (Figure 6D). There was a clear overlap of the $P2X_4$ immunolabelling and LAMP-1 in OHC (Figure 6D, Table 2).

GM130 is a marker for Golgi matrix protein of 130kDa, which typically targets the cis-component of Golgi (Nakamura, Lowe, Levine, Rabouille, & Warren, 1997). The Golgi apparatus is located mainly around the apical part of the cytoplasm in HCs (Schug et al., 2006; Spicer et al., 1998, 1999). In the rat cochlea, cytoplasmic expression of GM130 was observed in the IHCs and OHCs with vesicular, string-like structures (Figure 6E, F), consistent with previous reports (Schug et al., 2006). Notably, the co-occurrence of the GM130 and $P2X_4$ in both the IHCs and OHCs was minimal (Figure 6E, F), 11.7% ± 2.4%, and in the OHCs, 27% ± 2%. TOM20 is a protein expressed on the mitochondrial outer membrane (Balaker, Ishiyama, Lopez, Ishiyama, & Ishiyama, 2013) and was used here as the marker for mitochondria. There was some overlap of TOM20 and $P2X_4$ signal in the IHCs (Figure 6G, arrow). However, there was little co-localization between $P2X_4$ and TOM20 in both OHCs and IHC (Figure 6H). TOM20 was co-occurred with $P2X_4$ in the IHCs 13.7% ± 2.5% and in OHCs 11.3% ± 1.2%. Finally, WGA is naturally occurring molecule known to bind to glycoproteins found in the cell membrane, and fluorescent conjugates are commonly used as a marker for cell membrane (Emde, Heinen, Gödecke, & Bottermann, 2014). The WGA labelled the OHC membrane but did not stain IHC, similar to a previous study (Gil-Loyzaga & Brownell, 1988). Therefore, the association with the IHC membrane was inconclusive and therefore not included in this study. We observed the minimal overlap between WGA and $P2X_4$ in the OHCs(Figure 6I). WGA was co-localized with $P2X_4$ in OHCs 4.3% ± 0.2% (Figure 6K).

In summary, in IHCs, EEA-1 and GM130 have the highest percentage of co-localization with $P2X_4$, at 26% and 27%, respectively, compared to other organelle markers, suggesting cytoplasmic $P2X_4$ were likely associated with endosomes and Golgi apparatus. The co-localization pattern in OHCs was slightly different from that with IHCs; EEA-1 and LAMP-1 have a higher percentage of co-localization with $P2X_4$ at 42.3% and 32.%, respectively. This suggests that $P2X_4$ associate with endosomes and lysosomes in OHCs (Figure 6 K&L, Table 2).

DISCUSSION

In this study, we have comprehensively mapped the expression of $P2X_4$ in the Wistar rat cochlea using immunohistochemistry and reported the expression in the IHCs and OHCs of the Wistar rat cochlea for the first time. The minimal expression of $P2X_4$ labelling in the stria vascularis was unexpected, as the literature suggested that $P2X_4$ receptors are expressed in the endothelial cells of spiral ligament capillaries in the lateral wall of the guinea pig cochlea (Y. Wu et al., 2011). This discrepancy might occur because different antibody from Abcam (UK) was used, which is no longer available on the manufacturer website. The expression of $P2X_4$ in sensory HCs was observed uniformly throughout the apical, middle and basal turn of the cochlea (Supplementary Figure 4). $P2X_4$ immunolcalisation was observed in a small population of cells in the spiral ligament and the spiral ganglia, however, the frequency was very low in the adult cochlea.

It is important to note that the $P2X_4$ subunit can form heteromeric channels with $P2X_{1,\ 5,\ 6,\ and\ 7}$ subunits. $P2X_4$ immunolocalisationin the OoC in our study is distinctively different from what has been reported for $P2X_1$ (Xiang, Bo, & Burnstock, 1999), $P2X_7$ (Predrag Nikolic et al., 2003) and $P2X_2$ (Jarlebark et al., 2000; J. C. C. Wang et al., 2003), which might suggest that $P2X_4$ has different roles compared to other isoforms. The most intense $P2X_4$ expression was observed in the IHCs and OHCs, where $P2X_4$ was predominately localised in the cytoplasm with distinct polarity in the subcellular distribution of the receptor protein. Using organelle markers, we show that the majority of cytoplasmic $P2X_4$ was co-localized with vesiculated structures, particularly early endosomes and Golgi (trans-Golgi network), which combined represented 53% of the co-localisation for IHCs and 63.2 % for OHCs. Additional association with lysosomes occurred in OHCs only. There was little evidence of $P2X_4$ expression in the cell plasma membrane.

The cytoplasm of IHCs and OHCs are enriched with endosomes (Spicer et al., 1998, 1999). This $P2X_4$ localisation may represent a pool of $P2X_{4,}$ which will become inserted into the membrane under certain conditions, or it reflects continual membrane-cytoplasm cycling. Cytoplasmic $P2X_4$ has been reported in many tissues, including alveolar epithelium, and neurons (Bobanovic, Royle, & Murrel-Lagnoado, 2002; Qureshi, Paramasivam, Yu, & Murrell-Lagnado, 2007; Stokes, Layhadi, Bibic, Dhuna, & Fountain, 2017). In the ocular lens, cytoplasmic $P2X_4$ becomes more associated with the cell membrane under osmotic stress (Suzuki-Kerr, Lim, Vlajkovic, & Donaldson, 2009), supporting the notion that cytoplasmic vesicles containing $P2X_4$ are dynamic. Interestingly, the distribution of cytoplasmic $P2X_4$ showed polarity within the cell. The apical cell domain of both OHCs and IHCs are in contact with potassium-rich endolymphatic fluid, whereas the basal-lateral domain is in contact with sodium-rich perilymph and has the pre-synaptic clefts for synaptic transmission. A large proportion of cytoplasmic $P2X_4$ immunolabeling in the IHCs occurred on the apical and basal ends, in proximity to the synaptic cleft, which may suggest physiological $P2X_4$ roles in regulating pre-synaptic function. In addition, the cytoplasmic labelling in the IHCs was concentrated adjacent to the medial side of the lateral membrane. The medial side of IHCs is adjacent to the inner border cells, which abundantly express connexin 26 and 30, and while their primary role is communication between supporting cells as gap junctions, they also exist as connexin hemichannels (Taylor, Jagger, & Forge, 2012; Zhao, Yu, & Fleming, 2005). It is interesting to speculate that $P2X_4$ may be activated in a paracrine manner by connexin hemichannel-mediated ATP released

from the inner border cells. Such a gradient of $P2X_4$ distribution in the IHCs was not observed in younger animals (P4-P8), suggesting that $P2X_4$ signalling may be established in mature IHCs.

OHCs are the other type of sensory epithelial cells in the cochlea, however, they have distinct functional role than IHCs as part of the 'cochlear amplifier' by contracting and elongating in response to sound (Pickles, 1998). The robust expression of $P2X_4$ was found in OHCs mainly in the cytoplasmic space near the apical membrane and also towards the basal membrane. This was less evident in young animals, suggesting critical roles for $P2X_4$ in more mature OHCs. The large proportion (63.2%) of cytoplasmic $P2X_4$ in OHCs co-occurred with trans-Golgi network similar to the IHCs, and this may represent the dynamic cycling pool of $P2X_4$ receptors moving to and from the plasma membrane. Given the close proximity of vesicular $P2X_4$ to the apical and basal membranes, we may speculate ATP released from Deiters cells underneath OHCs which express connexin 26 and 30, proteins capable of forming hemi-channels and gap-junctions (Hosoya et al., 2021; Taylor et al., 2012; Zhao et al., 2005). In addition to the robust basal expression, both qualitative and quantitative analysis showed a robust $P2X_4$ expression at the apical sub-cuticular level of the OHCs, where they exhibited very characteristic appearance of "plaque" or "cluster" of vesicles. These were often found immediately underneath the CP free zone. While only 11.7% of $P2X_4$ co-localized in IHCs with the lysosome marker, a greater proportion (32.4%) of $P2X_4$ co-localized with lysosome marker in OHCs, showing differences between IHCs and OHCs. One possibility for lysosomal localization of $P2X_4$ is a part of protein cycling; the late-endosome will fuse with lysosome during protein degradation, some of which may correspond to $P2X_4$ receptors trafficking *en route* for degradation. Alternatively, $P2X_4$ has been suggested to play a role as a lysosomal ionic channel based on the observation in cultured neurons (R. D. Murrell-Lagnado, 2018; Ruth D. Murrell-Lagnado & Frick, 2019). Lysosomal $P2X_4$ receptor activation is influenced by pH within the lysosome lumen in cell culture and induces membrane fusion (Cao et al., 2015). In the cochlea, lysosomal dysfunction has been reported to lead to cellular toxicity in OHCs but not in IHCs (Wiwatpanit et al., 2018). It would be interesting to explore the difference in lysosomal physiology between IHCs and OHCs, and how $P2X_4$ in OHC lysosomes may be involved in such a process. Understanding the role of $P2X_4$ will require further investigation into the physiological activation of $P2X_4$, including pharmacological manipulations. $P2X_4$ receptor signalling and its intracellular roles in the cochlea likely contribute to the sensory cell physiology and pathophysiology.

Abbreviations

ADP – adenosine 5'-diphosphate

ATP – adenosine 5'-triphosphate

BDNF – Brain-derived neurotrophic factors

Ca^{2+} – calcium ion

dB – decibels

EP – endocochlear potential

IHCs – inner hair cells

JACoP – Just Another Co-localization Plugin (ImageJ plugin)

K^+ – potassium ion

kHz – Kilohertz

mM – micromolar

Mo – modiolus

OHCs – outer hair cells

OoC – organ of Corti

ROI – Region of interest

SGN – spiral ganglion neuron

SNHL – Sensorineural hearing loss

SV – stria vascularis

UDP – uridine diphosphate

UTP – uridine triphosphate

v/v – volume per volume

w/v – weight per volume

WGA – wheat germ agglutin

WHO – World Health Organization

Declarations

ACKKNOWLEDGEMENTS

This work was supported by the Auckland Medical Research Foundation (New Zealand) and Eisdell Moore Centre (New Zealand). Embryonic cochlea issue (E20) was supplied as a by-product from another AEC-approved study conducted by Dr. Rashika Karunasinghe (Department of Physiology, the University of Auckland, AEC 1977).

CONFLICTS OF INTERESTS

The authors declare that they have no conflict of interest.

AUTHOR CONTRIBUTIONS

HSK conceptualized and designed the study. ZH performed the majority of experiments, followed by HSK performing parts of the experiment. KR contributed to experiments in Figure 2. Technical protocols for optimization of the experiment, image acquisition and image analyses were designed and optimized by ZH, HSK, JMR, and SCY, followed by ZH conducting the data analysis. HSK and ZH wrote the draft of the manuscript. SMV and PRT were co-supervisors to ZH during her postgraduate degree and provided scientific guidance to the manuscript. ZH and HSK prepared figures. All authors have reviewed and approved the manuscript.

References

1. Balaker, A. E., Ishiyama, P., Lopez, I. A., Ishiyama, G., & Ishiyama, A. (2013). Immunocytochemical localization of the translocase of the outer mitochondrial membrane (Tom20) in the human cochlea. *The Anatomical Record, 296*(2), 326-332.
2. Bobanovic, L. K., Royle, S. J., & Murrel-Lagnoado, R. D. (2002). P2X Receptor Trafficking in Neurons Is Subunit Specific. *The Journal of Neuroscience, 22*(12), 4814-4824.
3. Bolte, S., & Cordelières, F. P. (2006). A guided tour into subcellular colocalization analysis in light microscopy. *Journal of microscopy, 224*(3), 213-232.
4. Burnstock, G. (1997). The past, present and future of purine nucleotides as signalling molecules. *Neuropharmacology, 36*(9), 1127-1139.
5. Burnstock, G. (2007). Purine and pyrimidine receptors. *Cellular & Molecular Life Sciences, 64*(12), 1471-1483.
6. Cao, Q., Zhong, X. Z., Zou, Y., Murrell-Lagnado, R., Zhu, M. X., & Dong, X.-P. (2015). Calcium release through P2X4 activates calmodulin to promote endolysosomal membrane fusion. *Journal of Cell Biology, 209*(6), 879-894.
7. Dunn, K. W., Kamocka, M. M., & McDonald, J. H. (2011). A practical guide to evaluating colocalization in biological microscopy. *American Journal of Physiology-Cell Physiology, 300*(4), C723-C742.
8. Emde, B., Heinen, A., Gödecke, A., & Bottermann, K. (2014). Wheat germ agglutinin staining as a suitable method for detection and quantification of fibrosis in cardiac tissue after myocardial infarction. *European journal of histochemistry: EJH, 58*(4)
9. Fok, C., Bogosanovic, M., Pandya, M., Telang, R., Thorne, P. R., & Vlajkovic, S. M. (2020). Regulator of G protein signalling 4 (RGS4) as a novel target for the treatment of sensorineural hearing loss. *International Journal of Molecular Sciences, 22*(1), 3.
10. Gil-Loyzaga, P., & Brownell, W. E. (1988). Wheat germ agglutinin and Helix pomatia agglutinin lectin binding on cochlear hair cells. *Hearing research, 34*(2), 149-155.
11. Gindhart, J., & Weber, K. (2009). Lysosome and endosome organization and transport in neurons.
12. Goodyear, R. J., Marcotti, W., Kros, C. J., & Richardson, G. P. (2005). Development and properties of stereociliary link types in hair cells of the mouse cochlea. *The Journal of comparative neurology, 485*(1), 75-85.

13. Han, R. B., Lin, C. S., Espinosa, K., Thorne, R. P., & Vlajkovic, M. S. (2019). Inhibition of the Adenosine A2A Receptor Mitigates Excitotoxic Injury in Organotypic Tissue Cultures of the Rat Cochlea. *Cells, 8*(8) 10.3390/cells8080877
14. Hattori, M., & Gouaux, E. (2012). Molecular mechanism of ATP binding and ion channel activation in P2X receptors. *Nature, 485*(7397), 207-212.
15. Hosoya, M., Fujioka, M., Murayama, A. Y., Ogawa, K., Okano, H., & Ozawa, H. (2021). Dynamic spatiotemporal expression changes in connexins of the developing primate's cochlea. *Genes, 12*(7), 1082.
16. Huang, L.-C., Ryan, A. F., Cockayne, D. A., & Housley, G. D. (2006). Developmentally regulated expression of the P2X3 receptor in the mouse cochlea. *Histochemistry and cell biology, 125*(6), 681-692.
17. Huang, P., Zou, Y., Zhong, X. Z., Cao, Q., Zhao, K., Zhu, M. X., . . . Dong, X. P. (2014). P2X4 forms functional ATP-activated cation channels on lysosomal membranes regulated by luminal pH. *J Biol Chem, 289*(25), 17658-17667. 10.1074/jbc.M114.552158
18. Huotari, J., & Helenius, A. (2011). Endosome maturation. *The EMBO journal, 30*(17), 3481-3500.
19. Jarlebark, L. E., Housley, G. D., & Thorne, P. R. (2000). Immunohistochemical localization of adenosine 5'-triphosphate-gated ion channel P2X(2) receptor subunits in adult and developing rat cochlea. *The Journal of comparative neurology, 421*(3), 289-301.
20. Jeong, J., Kim, J. Y., Hong, H., Wangemann, P., Marcus, D. C., Jung, J., . . . Kim, S. H. (2020). P2RX2 and P2RX4 receptors mediate cation absorption in transitional cells and supporting cells of the utricular macula. *Hearing research, 386*, 107860.
21. Jung, J., Yoo, J. E., Choe, Y. H., Park, S. C., Lee, H. J., Lee, H. J., . . . Lee, K.-M. (2019). Cleaved cochlin sequesters pseudomonas aeruginosa and activates innate immunity in the inner ear. *Cell host & microbe, 25*(4), 513-525. e516.
22. Kishimoto, I., Okano, T., Nishimura, K., Motohashi, T., & Omori, K. (2019). Early development of resident macrophages in the mouse cochlea depends on yolk sac hematopoiesis. *Frontiers in neurology, 10*, 1115.
23. Köles, L., Szepesy, J., Berekméri, E., & Zelles, T. (2019). Purinergic Signaling and Cochlear Injury-Targeting the Immune System? *International Journal of Molecular Sciences, 20*(12), 2979.
24. Lalisse, S., Hua, J., Lenoir, M., Linck, N., Rassendren, F., & Ulmann, L. (2018). Sensory neuronal P2RX4 receptors controls BDNF signaling in inflammatory pain. *Scientific reports, 8*(1), 1-12.
25. Liberman, M. C., & Kujawa, S. G. (2017). Cochlear synaptopathy in acquired sensorineural hearing loss: Manifestations and mechanisms. *Hearing research, 349*, 138-147.
26. Morton-Jones, R. T., Vlajkovic, S. M., Thorne, P. R., Cockayne, D. A., Ryan, A. F., & Housley, G. D. (2015). Properties of ATP-gated ion channels assembled from P2X2 subunits in mouse cochlear Reissner's membrane epithelial cells. *Purinergic signalling, 11*(4), 551-560. https://dx.doi.org/10.1007/s11302-015-9473-4
27. Murrell-Lagnado, R. D. (2018). A role for P2X(4) receptors in lysosome function. *J Gen Physiol, 150*(2), 185-187. 10.1085/jgp.201711963
28. Murrell-Lagnado, R. D., & Frick, M. (2019). P2X4 and lysosome fusion. *Current Opinion in Pharmacology, 47*, 126-132. https://doi.org/10.1016/j.coph.2019.03.002
29. Nakamura, N., Lowe, M., Levine, T. P., Rabouille, C., & Warren, G. (1997). The vesicle docking protein p115 binds GM130, a cis-Golgi matrix protein, in a mitotically regulated manner. *Cell, 89*(3), 445-455.

30. Nikolic, P., Housley, G. D., Luo, L., Ryan, A. F., & Thorne, P. R. (2001). Transient expression of P2X(1) receptor subunits of ATP-gated ion channels in the developing rat cochlea. *Brain research. Developmental brain research, 126*(2), 173-182.
31. Nikolic, P., Housley, G. D., & Thorne, P. R. (2003). Expression of the P2X7 receptor subunit of the adenosine 5'-triphosphate-gated ion channel in the developing and adult rat cochlea. *Audiology & neuro-otology, 8*(1), 28-37.
32. Organization, W. H. (2021). *World Report on Hearing*.
33. Patki, V., Virbasius, J., Lane, W. S., Toh, B.-H., Shpetner, H. S., & Corvera, S. (1997). Identification of an early endosomal protein regulated by phosphatidylinositol 3-kinase. *Proceedings of the National Academy of Sciences, 94*(14), 7326-7330.
34. Pickles, J. (1998). An introduction to the physiology of hearing *An Introduction to the Physiology of Hearing*: Brill.
35. Qureshi, O. S., Paramasivam, A., Yu, J. C., & Murrell-Lagnado, R. D. (2007). Regulation of P2X4 receptors by lysosomal targeting, glycan protection and exocytosis. *Journal of cell science, 120*(21), 3838-3849.
36. Robertson, D., & Paki, B. (2002). A role for purinergic receptors at the inner hair cell-afferent synapse? *Audiology and Neurotology, 7*(1), 62-67.
37. Schug, N., Braig, C., Zimmermann, U., Engel, J., Winter, H., Ruth, P., . . . Knipper, M. (2006). Differential expression of otoferlin in brain, vestibular system, immature and mature cochlea of the rat. *European Journal of Neuroscience, 24*(12), 3372-3380.
38. Sim, J. A., Chaumont, S., Jo, J., Ulmann, L., Young, M. T., Cho, K., . . . Rassendren, F. (2006). Altered hippocampal synaptic potentiation in P2X4 knock-out mice. *J Neurosci, 26*(35), 9006-9009. 10.1523/jneurosci.2370-06.2006
39. Smeti, I., Savary, E., Capelle, V., Hugnot, J. P., Uziel, A., & Zine, A. (2011). Expression of candidate markers for stem/progenitor cells in the inner ears of developing and adult GFAP and nestin promoter-GFP transgenic mice. *Gene Expression Patterns, 11*(1-2), 22-32.
40. Spicer, S. S., Thomopoulos, G. N., & Schulte, B. A. (1998). Cytologic evidence for mechanisms of K+ transport and genesis of Hensen bodies and subsurface cisternae in outer hair cells. *The Anatomical Record: An Official Publication of the American Association of Anatomists, 251*(1), 97-113.
41. Spicer, S. S., Thomopoulos, G. N., & Schulte, B. A. (1999). Novel membranous structures in apical and basal compartments of inner hair cells. *Journal of Comparative Neurology, 409*(3), 424-437.
42. Stokes, L., Layhadi, J. A., Bibic, L., Dhuna, K., & Fountain, S. J. (2017). P2X4 Receptor Function in the Nervous System and Current Breakthroughs in Pharmacology. *Frontiers in Pharmacology, 8*(291) 10.3389/fphar.2017.00291
43. Suzuki-Kerr, H., Lim, J., Vlajkovic, S., & Donaldson, P. (2009). Differential membrane redistribution of P2X receptor isoforms in response to osmotic and hyperglycemic stress in the rat lens. *Histochemistry and Cell Biology, 131*(6), 667-680.
44. Szücs, A., Szappanos, H., Tóth, A., Farkas, Z., Panyi, G., Csernoch, L., & Sziklai, I. (2004). Differential expression of purinergic receptor subtypes in the outer hair cells of the guinea pig. *Hearing research, 196*(1-2), 2-7.

45. Taylor, R. R., Jagger, D. J., & Forge, A. (2012). Defining the cellular environment in the organ of Corti following extensive hair cell loss: a basis for future sensory cell replacement in the Cochlea. *PloS one, 7*(1), e30577.
46. Vlajkovic, S. M., & Thorne, P. R. (2022). Purinergic Signalling in the Cochlea. *International Journal of Molecular Sciences, 23*(23), 14874.
47. Wang, J. C. C., Raybould, N. P., Luo, L., Ryan, A. F., Cannell, M. B., Thorne, P. R., & Housley, G. D. (2003). Noise induces up-regulation of P2X2 receptor subunit of ATP-gated ion channels in the rat cochlea. *Neuroreport, 14*(6), 817-823.
48. Wang, Z.-J., & Neuhuber, W. (2003). Intraganglionic laminar endings in the rat esophagus contain purinergic P2X2 and P2X3 receptor immunoreactivity. *Anatomy and embryology, 207*(4), 363-371.
49. Wang, Z., Jung, J. S., Inbar, T. C., Rangoussis, K. M., Faaborg-Andersen, C., & Coate, T. M. (2020). The purinergic receptor P2rx3 is required for spiral ganglion neuron branch refinement during development. *Eneuro, 7*(4)
50. Wiwatpanit, T., Remis, N. N., Ahmad, A., Zhou, Y., Clancy, J. C., Cheatham, M. A., & García-Añoveros, J. (2018). Codeficiency of lysosomal mucolipins 3 and 1 in cochlear hair cells diminishes outer hair cell longevity and accelerates age-related hearing loss. *Journal of Neuroscience, 38*(13), 3177-3189.
51. Wu, P.-z., O'Malley, J. T., de Gruttola, V., & Liberman, M. C. J. J. o. N. (2020). Age-related hearing loss is dominated by damage to inner ear sensory cells, not the cellular battery that powers them. *40*(33), 6357-6366.
52. Wu, P. Z., Liberman, L. D., Bennett, K., de Gruttola, V., O'Malley, J. T., & Liberman, M. C. (2019). Primary Neural Degeneration in the Human Cochlea: Evidence for Hidden Hearing Loss in the Aging Ear. *Neuroscience, 407*, 8-20. https://doi.org/10.1016/j.neuroscience.2018.07.053
53. Wu, Y., Karna, S., Choi, C. H., Tong, M., Tai, H.-H., Na, D. H., . . . Cho, H. (2011). Synthesis and biological evaluation of novel thiazolidinedione analogues as 15-hydroxyprostaglandin dehydrogenase inhibitors. *Journal of medicinal chemistry, 54*(14), 5260-5264. https://dx.doi.org/10.1021/jm200390u
54. Wyatt, L. R., Finn, D. A., Khoja, S., Yardley, M. M., Asatryan, L., Alkana, R. L., & Davies, D. L. (2014). Contribution of P2X4 receptors to ethanol intake in male C57BL/6 mice. *Neurochemical research, 39*(6), 1127-1139. 10.1007/s11064-014-1271-9
55. Xiang, Z., Bo, X., & Burnstock, G. (1999). P2X receptor immunoreactivity in the rat cochlea, vestibular ganglion and cochlear nucleus. *Hear Res, 128*(1), 190-196. https://doi.org/10.1016/S0378-5955(98)00208-1
56. Xiong, H., Chen, S., Lai, L., Yang, H., Xu, Y., Pang, J., . . . Zheng, Y. (2019). Modulation of miR-34a/SIRT1 signaling protects cochlear hair cells against oxidative stress and delays age-related hearing loss through coordinated regulation of mitophagy and mitochondrial biogenesis. *Neurobiology of Aging, 79*, 30-42.
57. Zhao, H.-B., Yu, N., & Fleming, C. R. (2005). Gap junctional hemichannel-mediated ATP release and hearing controls in the inner ear. *Proceedings of the National Academy of Sciences, 102*(51), 18724-18729.

Tables

Table 1. Antibodies used in this study. Relevant information was gathered from datasheets for each antibody.

Antibody	Company/ catalogue No.	Epitope	Dilution	Reactivity	Marker for	Reference
Anti-$P2X_4$, Rabbit IgG polyclonal	Alomone APR-002	C-terminus of mouse P2X4 isoform	1:1000	Mouse, rat and human		
Anti-SOX2, Mouse IgG monoclonal	Santa Cruz Biotechnology Inc. Sc-365823	Human SOX2 amino acids 170-201	1:100	Mouse, rat and human	Cochlear supporting cell nucleus	(Oesterle et al., 2007) (Smeti et al., 2011)
Anti-Myosin VIIa, Mouse IgG monoclonal	Santa Cruz Biotechnology Inc. sc-74516	N-terminus of human Myosin VIIa	1:50	Mouse, rat and human	Inner hair cells & Outer hair cells	(Xiong et al., 2019) (Jung et al., 2019)
Anti-LAMP-1, Mouse IgG monoclonal	Santa Cruz Biotechnology Inc. sc-20011	Adherent spleen cells of human origin	1:200	Mouse, rat and human	Lysosomes	(Spangenberg et al., 2019) (Oh et al., 2020)
Anti-EEA-1, Mouse IgG monoclonal	Santa Cruz Biotechnology Inc. sc-137130	N-terminus of human EEA1	1:200	Mouse, rat, human and monkey	Endosomes	(Kuszczyk et al., 2013) (Men et al., 2019)
Anti-GM130, Mouse IgG monoclonal	BD Biosciences 610822	Rat GM130 aa. 869-982	1:200	Human dog and mouse	Golgi	(Dandoy-Dron et al., 2003) (Zheng et al., 2010)
Anti-TOM20, Mouse IgG monoclonal	Santa Cruz Biotechnology Inc. sc-17764	Human Tom20	1:200	Mouse, rat and human	Mitochondria	(Balaker et al., 2012) (Xiong et al., 2019)
WGA Alexa 647 Conjugate	Thermofisher	Wheat Germ Agglutinin (WGA)	1:300	All	Plasma membrane	(Graveleau et al., 2005)

						(Cui et al., 2020)
Phalloidin Alexa 488	Thermofisher	Phalloidin	1:500	All	Cytoskeletal actin	

Table 2 is not available with this version.

Figures

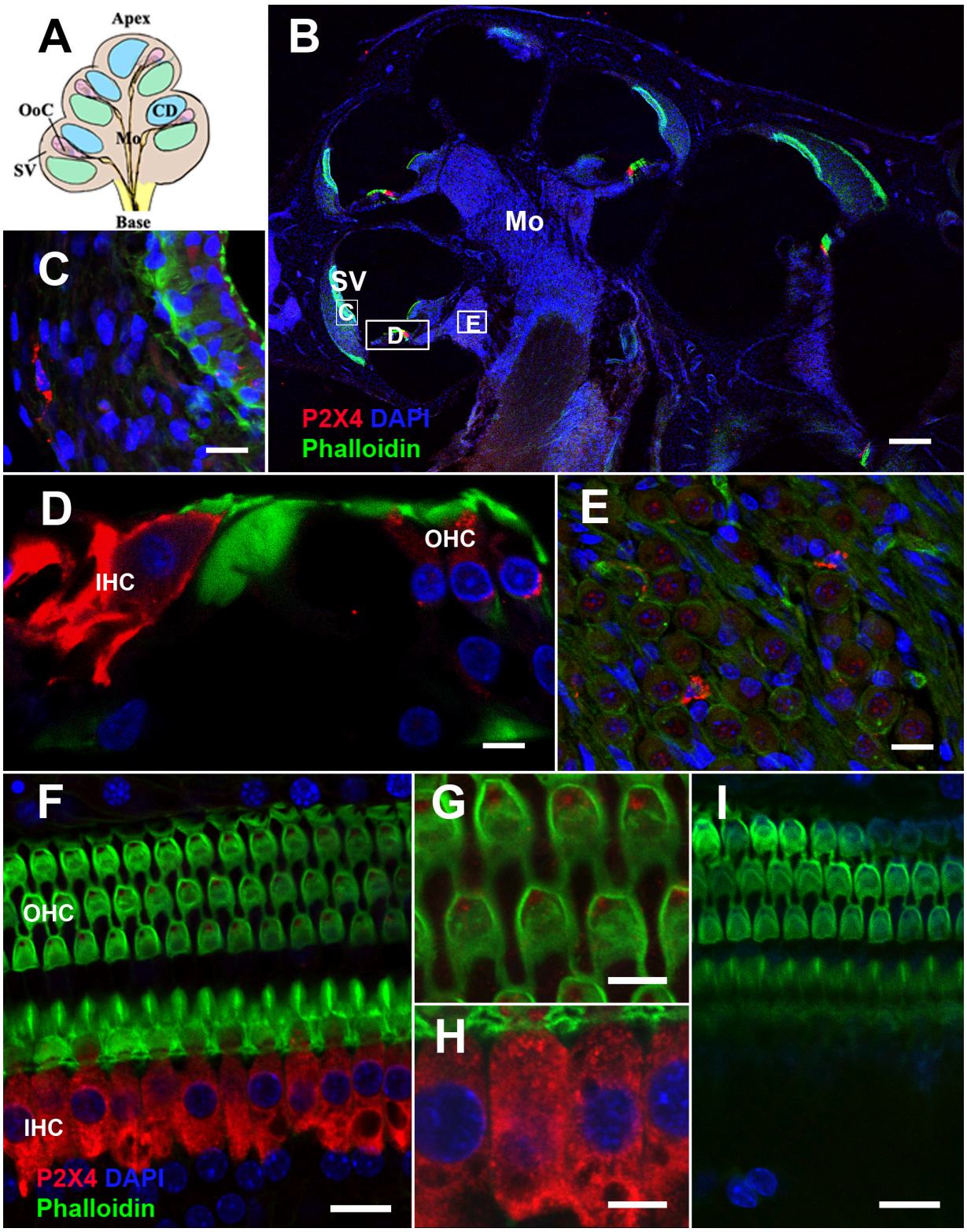

Figure 1

Expression of P2X4 in the adult rat cochlea. (A) Schematic drawing of OoC cryosection. **(B-I)** cryosections (B-E) and OoC wholemounts (F-I) were prepared from adult Wistar rat cochlea and labelled with anti-$P2X_4$ antibody (*red*), phalloidin (*green*) and DAPI (*blue*). (I) $P2X_4$ antibodies pre-absorbed with excess control peptide . Representative image from n=6 cochlea. Scale bar 200 µm (B), 20 µm (C, E, F, I), and 10 µm (D, G, H).

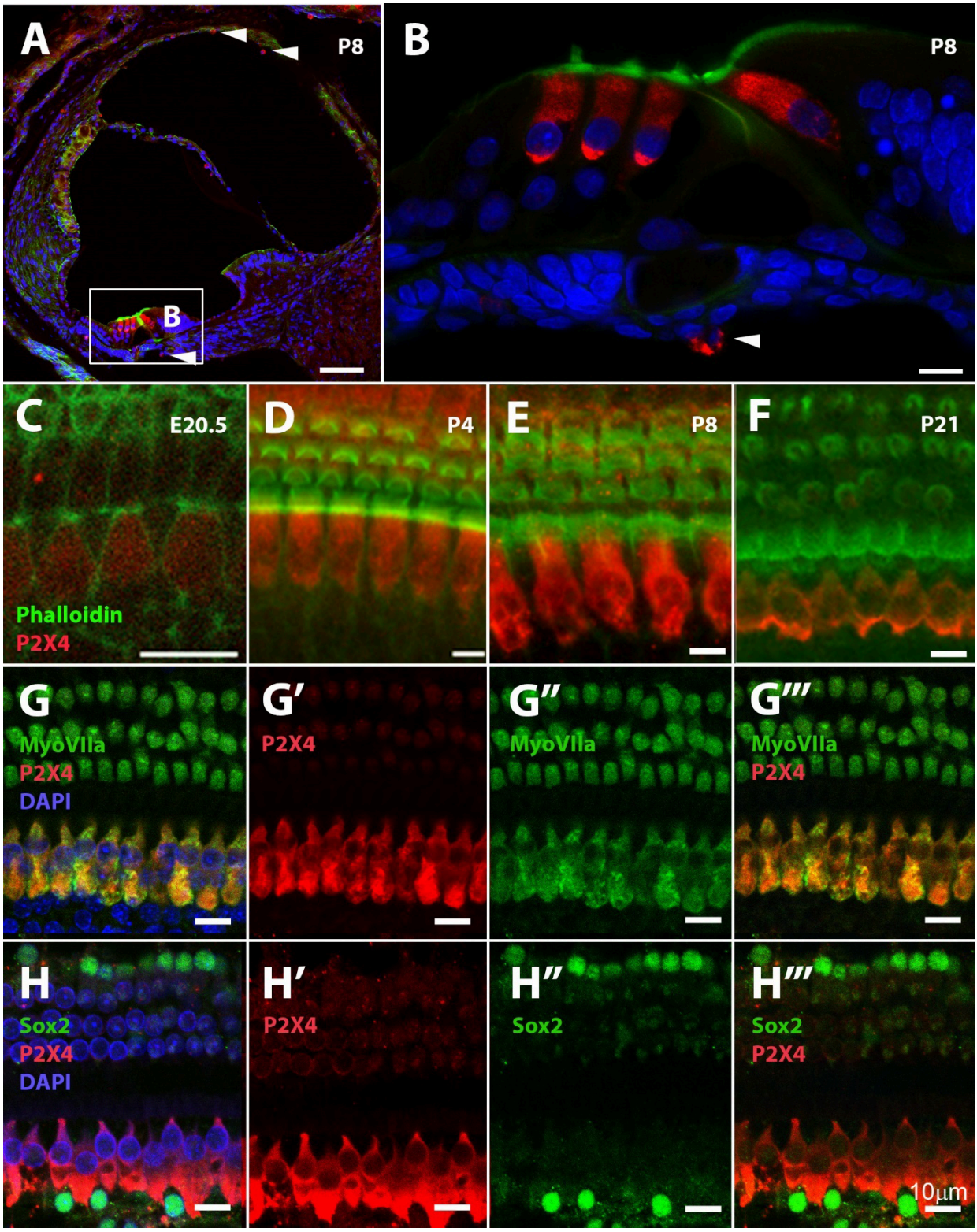

Figure 2

Developmental expression of $P2X_4$ in IHCs and OHCs. (A-F) Cryosection (A-B) and OoC whole mount preparation (C-F) of Wistar rat cochleae at P8 (A-B, E), E20.5 (C), P4 (D), P21 (F) labelled with anti-$P2X_4$ antibody (*red*) and phalloiding (*green*). **(G-H)** Adult cochlea whole mounts were labelled with anti-$P2X_4$ (*red*) and co-labelled with anti-MyosinVIIa (G, *green*) or anti-SOX2 (H, *green*) antibodies and DAPI (*blue*) in the OoC of the adult rat cochlea. Scale bar 50 µm (A) and 10 µm (B-H).

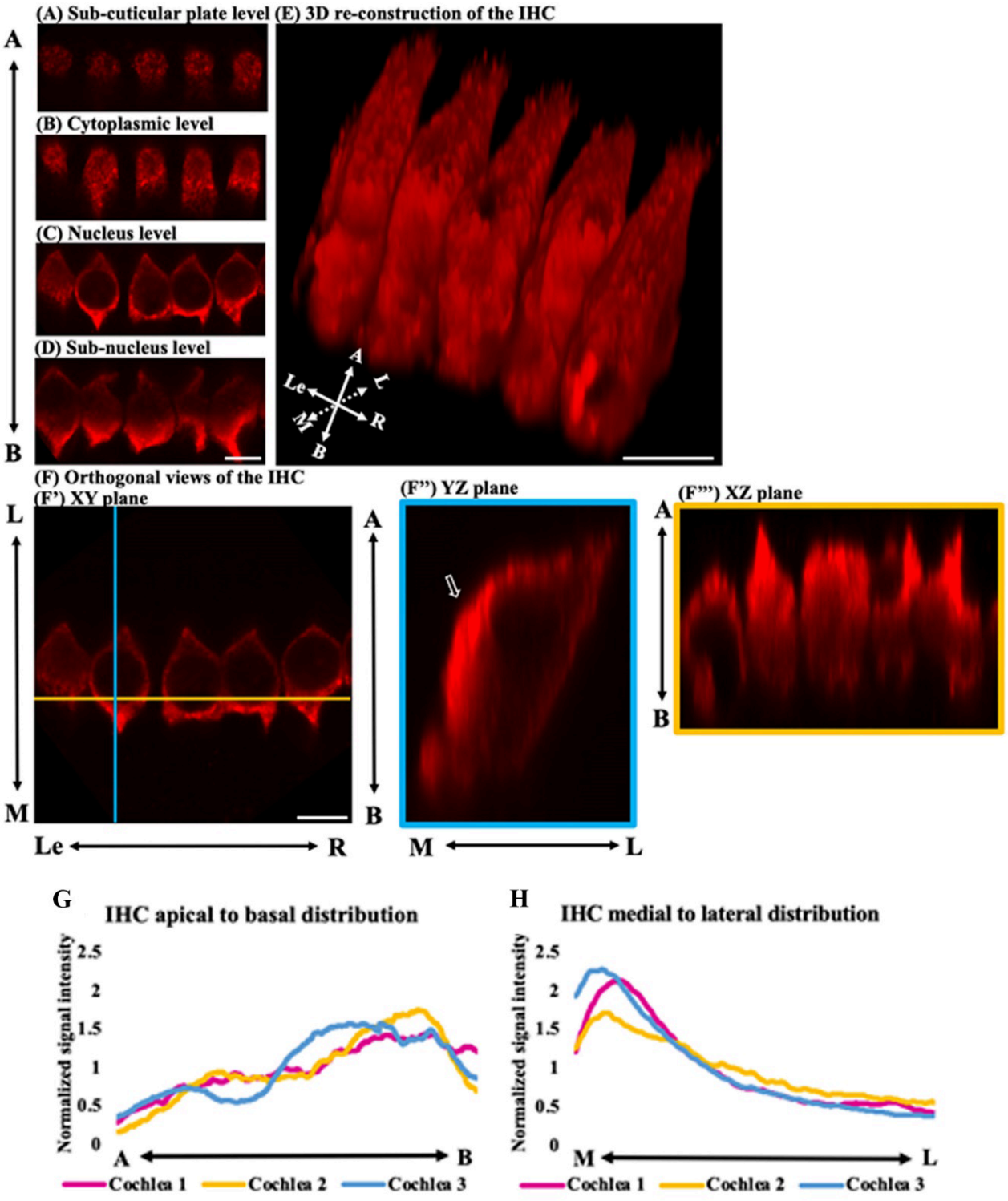

Figure 3

Subcellular distribution of $P2X_4$ in IHC. (A-D) The $P2X_4$ expression in the IHCs compared at different focal planes visualized by optical slicing along the z-axis. The axis on the left represents the images taken from the apical [A] to the basal [B] region of the cells. **(E)** The 3D reconstruction of the IHCs. The axis on the left bottom corner represents the cell orientation. **(F)** The orthogonal views of the IHCs with three planes shown XY plane (F'), YZ plane (F"), XZ plane (F"'). (Arrow) The bright $P2X_4$ signal at the medial end of the IHCs. Axis in the figure

are: [A] apical [B] basal [L] lateral (towards lateral wall side) [M] medial (towards modiolus side) [Le] left [R] right. Scale bars = 10mm. **(G & H)** $P2X_4$ normalized signal intensity (Y-axis) from 3 cochlea along the apical-basal axis (G) and medial-lateral axis (H). See Supplementary figure 5 and 6 for more information on the quantification. Axis in the figure are: [A] apical [B] basal [L] lateral (towards lateral wall side) [M] medial (towards modiolus side) [Le] left [R] right.

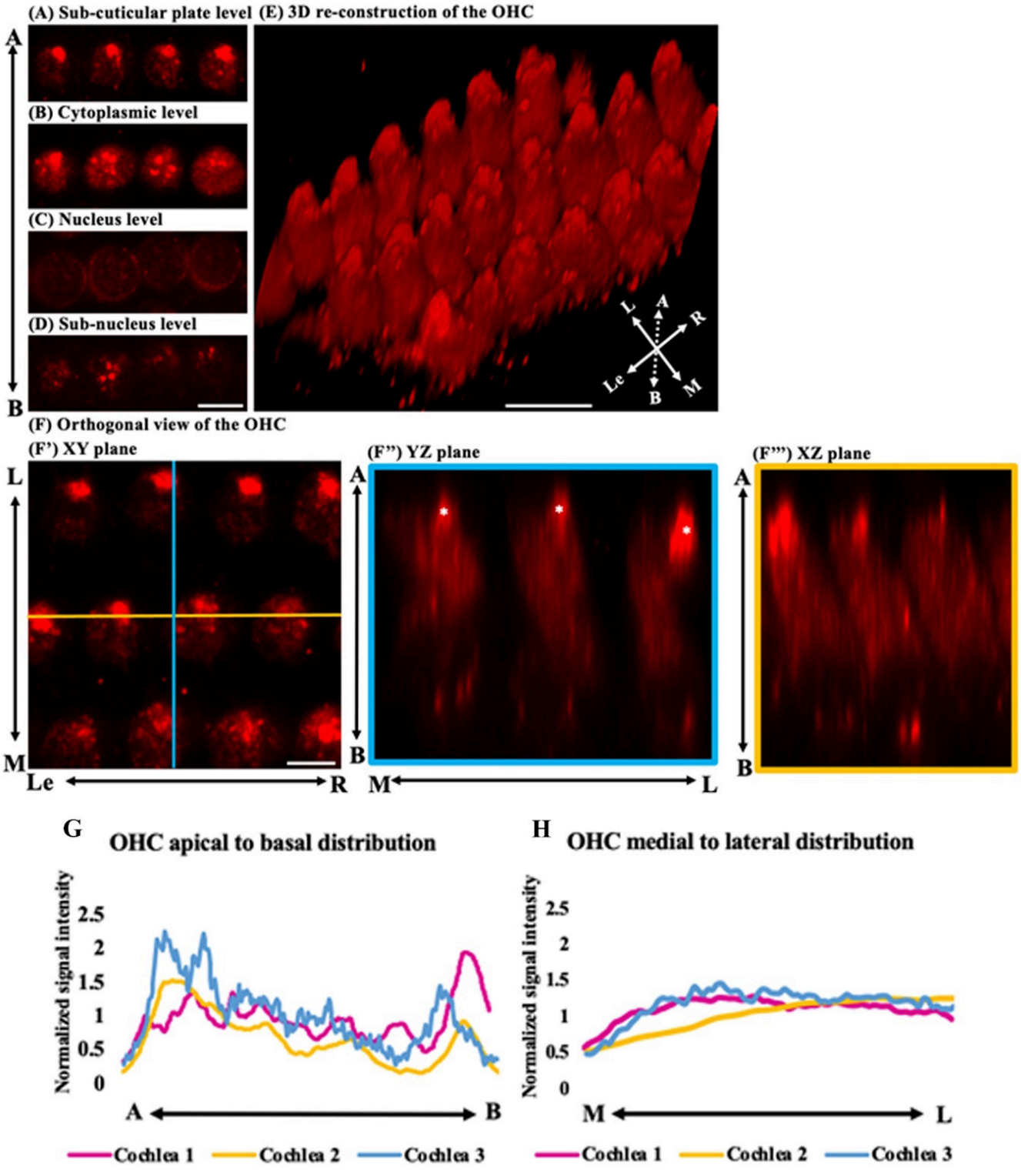

Figure 4

Subcellular distribution of $P2X_4$ in OHC. (A, B, C, D) The $P2X_4$ expression in the OHCs compared at different focal planes visualized by optical slicing along the z-axis. The axis on the left represents the images taken from the apical [A] to the basal [B] part of the cells. (E) The 3D reconstruction of the OHCs. The axis on the left bottom corner represents the cell orientation. (F) The orthogonal views of the OHCs with three planes shown as XY plane (F'), YZ plane (F''), XZ plane (F'''). (*) The prominent cluster of $P2X_4$ vesicles in the apical-lateral end of the OHCs. Axis in the figure are: [A] apical [B] basal [L] lateral (towards lateral wall side) [M] medial (towards modiolus side) [Le] left [R] right. Scale bars = 10mm. **(G & H)** $P2X_4$ normalized signal intensity (Y-axis) in 3 cochleae along the apical-basal axis (G) and along medial-lateral axis (H). See Supplementary figure 5 and 6 for more information on the quantification. Axis in the figure are: [A] apical [B] basal [L] lateral (towards lateral wall side) [M] medial (towards modiolus side) [Le] left [R] right.

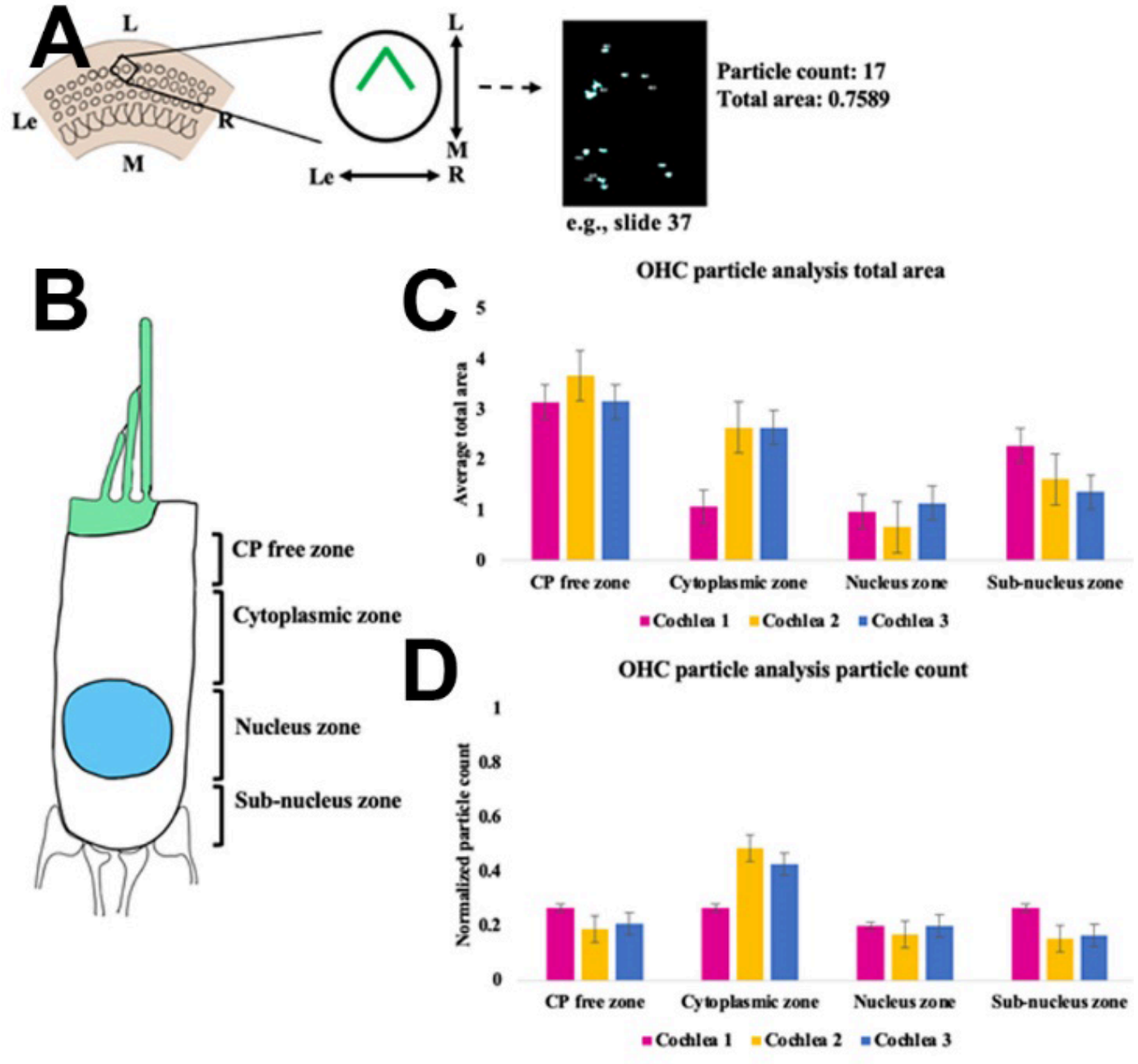

Figure 5

Particle analysis of $P2X_4$ immunolabeling in OHCs. (A) Schematic example of the selection of the cell and the particle analysis example. Each Z-stack of OHCs contains 70-90 optical sections depending on the plane of focus. Each slide in the Z-stack is displayed with particle counts and total area. **(B)** Schematic OHCs with the zone division. **(C)** The summary graph of the $P2X_4$ expression average total area and **(D)** normalized particle count. Axis in the figure is: [L] lateral (towards lateral wall side) [M] medial (towards modiolus side) [Le] left [R] right. Nine cells from three adult Wistar rats cochlea were subjected to the particle analysis.

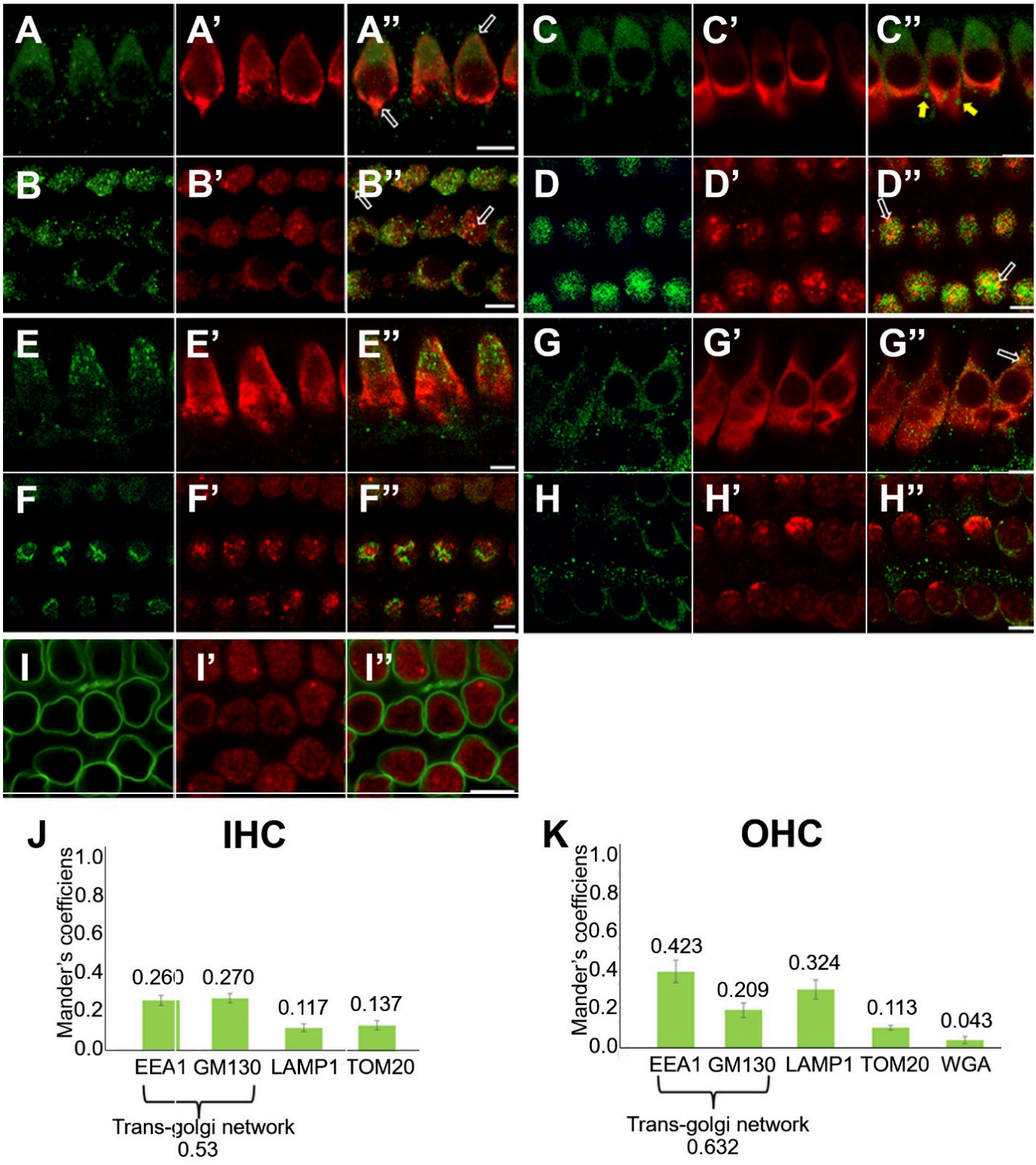

Figure 6

Co-localization of P2X4 in IHCs and OHCs with organelle markers. (A-J) OoC preparation from adult Wistar rats were immunolabelled with an anti-$P2X_4$ antibody (*red*) and one of the organelle markers (*green*); anti-EEA-1 (A-B), anti-LAMP-1(C-D), anti-GM130 (E-F), anti-TOM20 (G-H), WGA (I). High-resolution images were taken at IHC (A, C, E, G), and OHC (B, D, F, H, I). Open arrows indicate a double-positive signal, while closed arrows indicate a single-positive marker signal. Scale bars = 10µm. **(J-K)** Quantification of the co-localization of $P2X_4$ and organelle markers in IHCs (J) and OHCs (K) using JACoP ImageJ Plugin and Mander's coefficient (value range 0-1.0) has been summarised. n=3 cochleae were examined.

Supplementary Files

This is a list of supplementary files associated with this preprint. Click to download.

- HuangetalSupplementarymaterialv3.docx